

Geometrical importance sampling in Geant4: from design to verification

Michael Dressel *

CERN, CH-1211 Geneva 23, Switzerland

Abstract

The addition of flexible, general implementations of geometrical splitting and Russian Roulette, in combination called geometrical importance sampling, for variance reduction and of a scoring system, for controlling the sampling, are described. The efficiency of the variance reduction implementation is measured in a simulation of a typical benchmark experiment for neutron shielding. Using geometrical importance sampling a reduction of the computing time of a factor 89 compared to the analog calculation, for obtaining a neutron flux with a certain precision, was achieved for the benchmark application.

Key words: Geant4, Variance reduction, Importance sampling, Splitting, Russian Roulette

PACS: 02.50.N

**Email address:* michael.dressel@cern.ch (Michael Dressel).

Contents

1	Introduction	3
2	Variance reduction techniques	3
2.1	Geometrical importance sampling	4
3	Design	6
3.1	Requirements	6
3.2	Geometries	7
3.3	Sampler	7
3.4	Definition of cells	7
3.5	Importance value definition	9
3.6	Scoring	10
3.7	Outline of lower level concepts	12
4	Verification	13
4.1	Brief description of the experiment	13
4.2	Geant4 simulation of the TIARA experiment	14
4.3	The setup for the geometrical importance sampling	16
4.4	Results and FOM comparison for analog and non-analog calculations	17
4.5	Discussion of the results	20
4.6	Effect of detector resolution	28
5	Conclusion	29
	References	30

1 Introduction

Geant4 is a toolkit for the simulation of particle transport and their interactions with matter. The article [1] provides an overview of Geant4. The Geant4 homepage may be found currently at: <http://geant4.web.cern.ch/geant4>. Geant4 is used in a wide range of applications from high energy physics application, e.g. by the BABAR collaboration [2], to low energy medical applications (see e.g. [3] and [4]).

Variance reduction techniques [5] are used to save computing time in the estimation of the uneasy observables in the most computing-intensive Monte-Carlo simulations. Geometrical importance sampling is a well known variance reduction technique (see e.g. [6], [7]) typically applied in shielding, deep penetration, radiation and similar studies.

The simulation of neutrons and gammas penetrating deep into material is very time consuming as neutrons and gammas may be scattered many times and produce secondary radiation before being absorbed in the material. To reduce the computing time for calculations of neutron and gamma transport by Monte-Carlo methods, variance reduction techniques have been developed.

Section 2 gives a basic description of variance reduction techniques. A detailed description may be found in [8]. The implementation of the geometrical importance sampling in Geant4 is described in section 3. The properties of the importance sampling technique is investigated in section 4 by comparing simulations using the variance reduction technique with data from the neutron shielding benchmark experiment TIARA [9] and with the analog calculation.

2 Variance reduction techniques

A Monte-Carlo simulation is denoted analog if the possible outcomes of measurements to the estimator of an observable occur with the same frequencies as they do in nature. Variance reduction techniques change the sampling procedure. They aim to sample important contributions to the estimator more often than less important contributions. The Monte-Carlo is then said to be non-analog since it does not reflect the physical probabilities. The “bias” introduced by using a non-analog Monte-Carlo is taken into account by changing the weight of each measurement contributing to the estimator of the observable. The geometrical importance sampling used in this report and a variety of other variance reduction techniques may be found in the literature (see e.g. [8]) and are implemented in Monte-Carlo codes already. In [10] several variance reduction techniques implemented in MCNP [11] are demonstrated. Geometrical importance sampling is proved [8] not to bias the mean value of an estimator but to reduce its variance if it is applied correctly.

Since the goal of a variance reduction technique is to reduce computing time, the efficiency (see [8]) of such a technique is determined by the computing time and the precision achieved. Following the nomenclature used by MCNP this efficiency is called “feature of merit” (FOM). It is defined as:

$$FOM = \frac{1}{R^2 T} \quad (1)$$

where $R = \frac{\sigma}{\bar{x}\sqrt{N}}$ is the relative error of a quantity with mean value \bar{x} , standard deviation σ and N the number of measurements (e.g events or started tracks), T is the corresponding computing time.

2.1 Geometrical importance sampling

In this section the principals of the techniques geometrical splitting and Russian Roulette (see e.g. [5]) are outlined by considering a typical use case: The estimation of radiation flux through a detector where the radiation is produced in a source separated from the detector by a thick radiation absorbing shield.

Geometrical splitting

The idea behind geometrical splitting is to compensate for the exponential depletion of tracks in absorbing material by enhancing the number of independent tracks after certain distances of penetration towards important regions, e.g. a detector. Therefore, increasing the number of calculations with potentially important contributions to the quantities evaluated by the detector. A well known realisation of the technique, that is adopted by Geant4, is based on importance values assigned to cells of the geometry. A simple example is depicted in figure 1. Splitting occurs on the boundaries between cells when a particle moves in the direction of

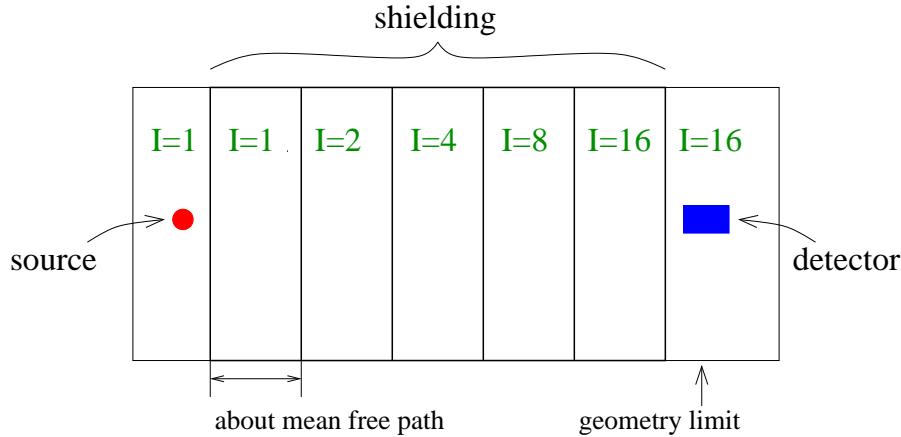


Figure 1: *Layout of a simple geometry subdivided into cells with importance values assigned to all cells. A source is separated by a shield from a detector. In the shield region the importance values, I , of the cells increase towards the detector. Importance values are assigned to every cell of the geometry.*

increased importance. Copies of the current track are created. The copies are tracked from the point of splitting instead of starting from the source therefore saving calculations in the less important cells.

The importance values of cells should typically be chosen such that they increase by factors of around two from cell to cell towards the detector. In this case the size of the cells along the path source-detector should typically be about the radiation length of the material (see e.g. [10]).

The surfaces splitting occurs on are defined in Geant4 by the boundaries of geometrical cells. The number of tracks created is determined by a well known algorithm according to the importance values assigned to the cells. In order not to bias the results to be estimated by the detector the weight of the tracks have to be adjusted appropriately.

Russian Roulette

Whereas splitting enhances the calculation of important contributions to a detector, the

Russian Roulette technique is used to reduce the calculation of unimportant contributions. Tracks crossing the surfaces in the direction of reduced importance are killed with a probability given by an algorithm according to the importance values of the cells. The weight of surviving particles is appropriately raised to prevent a bias of the results.

Algorithm for geometrical splitting and Russian Roulette

The exact behaviour of importance sampling may be defined in different ways by applying slightly different algorithms. The implementation described in section 3 supports customised algorithms and also provides an algorithm sometimes characterised as “expected value splitting” (see e.g. [11]). For a track with weight W crossing from cell m to cell n with the importance values I_m and I_n respectively, the algorithm works as follows:

1. Decide about applying splitting or Russian Roulette according to $r = I_n/I_m$:

- If $r = 1$: continue transport.
- If $r < 1$: play Russian Roulette, with r as the survival probability.
- If $r > 1$: determine the total number of tracks N after splitting:
 - r is an integer: $N = r$.
 - r is not an integer: two values for N are possible:
 - * $N = \text{int}(r) + 1$; with probability $p = r - \text{int}(r)$.
 - * $N = \text{int}(r)$; with probability $1 - p$.

2. Set the weights of all tracks to: $W \rightarrow \frac{W}{r}$ (expected value splitting).

The algorithm only ensures conservation of the statistical weight in the limit of an infinite number of events. Event-by-event the statistical weight is not conserved. Variance reduction techniques can be combined and the particle weight may therefore be changed by other techniques too. If, nevertheless, importance sampling using the above algorithm is the only weight changing source in the Monte-Carlo simulation the weight of every track in a cell i with importance I_i will be the same: $W = \frac{W_0}{I_i}$, with W_0 representing a possible initial weight of the track.

Figure 2 shows an example of geometrical splitting and Russian Roulette for tracks crossing between two cells with importance values different by a factor of two.

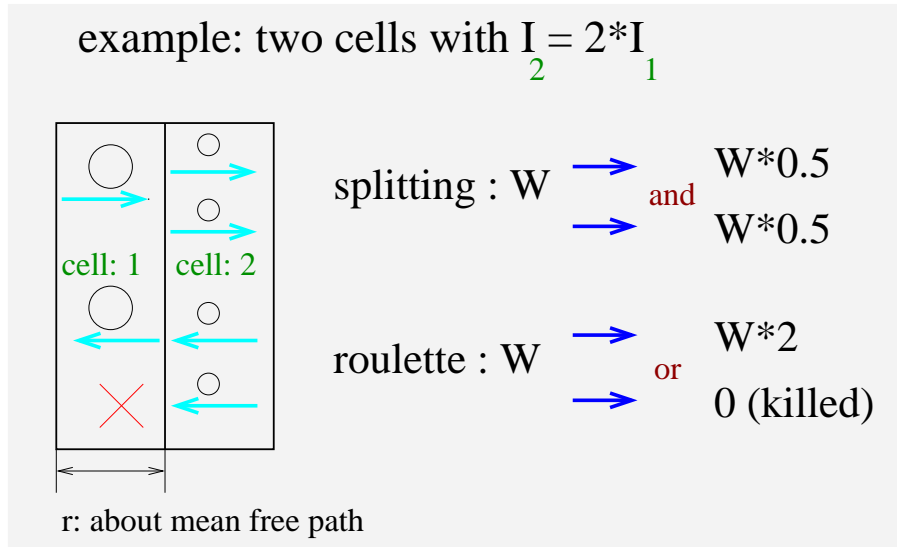


Figure 2: Example showing the behaviour of geometrical splitting and Russian Roulette for particles crossing between two cells. The importance values I_1 and I_2 of cell₁ and cell₂ in this example are related by: $I_2 = 2 * I_1$.

If a particle moves from cell 1 to cell 2 it will be split in two particles and the weight of the two particles will be half of the weight of the incoming particle. If a particle moves from cell 2 to cell 1 Russian Roulette will be played with a survival probability of 50 %. The particle will either be killed or its weight will be doubled and it will be tracked further.

3 Design

The requirements determining the design are given in section 3.1. The following sections describe the user level classes in a top to bottom view and give some rationals for the design decisions taken. Sections 3.2, 3.3 and 3.4 describe basic concepts common to importance sampling and scoring. In the sections 3.5 and 3.6 concepts of the implementation of importance sampling and scoring are given respectively. Lower level concepts needed for the implementation are outlined in section 3.7 briefly without showing all the details.

3.1 Requirements

The goal of the implementation is the speeding up of computing intensive calculations like shielding against neutrons typically with energies of a few MeV and below. The implementation should provide basic scoring. The scoring produces quantities allowing to control the importance sampling and aiding in the optimisation of the importance configuration, e.g. defining the geometry cells and choosing importance values. The most important requirements for importance sampling and scoring are:

1. The geometry representing the experiment and additional specialised geometries should be supported by importance sampling and scoring.
2. Provide the possibility to assign different importance values for different particle types.

3. One geometry may be used for one or more particle types.
4. Multiple geometries may be used for different particle types.
5. Scoring may be used independent of importance sampling.
6. The importance sampling as well as the scoring is currently required only for neutral particles. Thus magnetic fields don't need to be supported.

3.2 Geometries

The geometry representing the experiment, called mass geometry, is used in Geant4 for transporting particles by taking their physical interactions with matter into account. The mass geometry does not necessarily provide the most suitable geometry for importance sampling and scoring. Therefore the use of alternative geometries, called parallel geometries, are supported by the implementation of importance sampling and scoring. The parallel geometries are made of the same components as the mass geometry, only that the materials assigned to their volumes are not considered. Since parallel geometries are technically equivalent to the mass geometry they may be tested or visualised in the same way as the mass geometry. Note that parallel geometries are not taken into account by the usual transportation in Geant4.

Importance sampling and scoring is done on a per-particle type basis. Consequently, different geometries may be used for different particle types. On the other hand, it is also possible to use one geometry for several particle types.

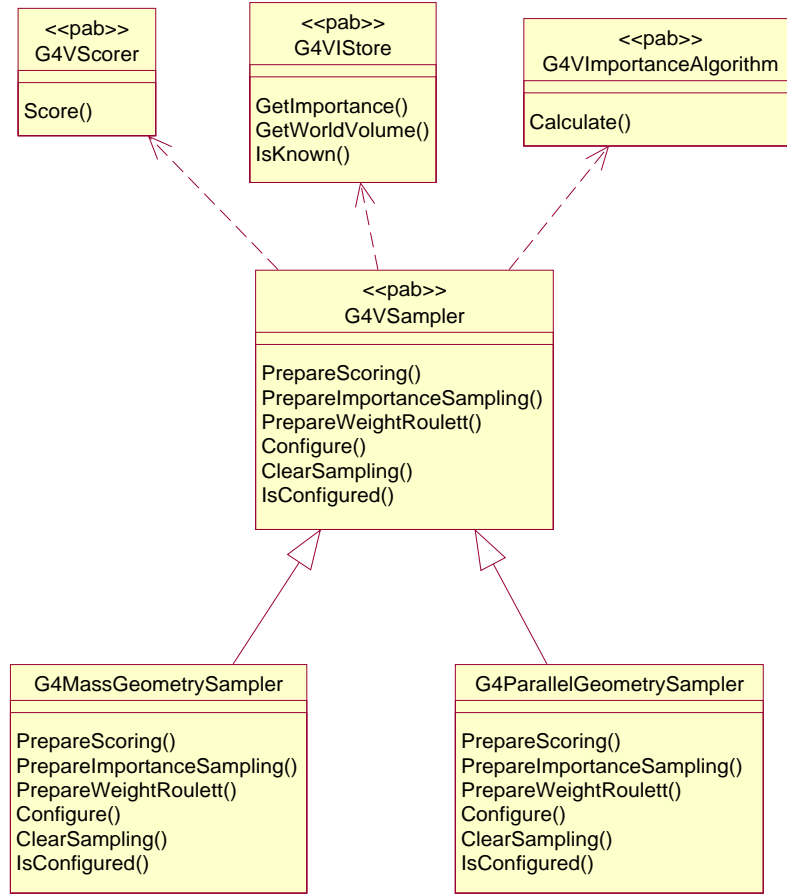
3.3 Sampler

Importance sampling and scoring are introduced into the Geant4 simulation with a top-level concept defined by the interface class *G4VSampler* (see figure 3). Concrete classes implementing this interface configure the simulation with the importance values defined by the user and allow customised scorers and algorithms for geometrical splitting and Russian Roulette to be applied during the simulation. Supported customised scorers, importance stores and optional importance algorithms must derive from the interface classes *G4VScorer* (see section 3.6), *G4VStore* and *G4VImportanceAlgorithm* (see section 3.5) respectively. Default realisations of these interfaces are also provided.

The implementation of the interface class *G4VSampler* is much more simple for the samplers responsible for the mass geometry than for samplers for parallel geometries since the necessary informations and services are provided by the Geant4 kernel for the mass geometry already. Therefore, the two different classes *G4MassGeometrySampler* and *G4ParallelGeometrySampler* have been implemented. See section 3.7 for the additional implementation needed for the parallel geometries.

3.4 Definition of cells

In Geant4 a physical volume (*G4VPhysicalVolume*) describes a volume placed at a certain position in the geometry and related to a logical volume, *G4LogicalVolume*. Geant4 provides the concept of replication to have one physical volume represent several volumes at different positions. These replicas are distinguished from each other by a replica number a



pab: purely abstract base class

Figure 3: The top-level interface class *G4VSampler* provides for setting up the importance sampling and scoring. For the mass and parallel geometries different concrete classes *G4MassGeometrySampler* and *G4ParallelGeometrySampler* are provided.

translation and their position in the geometry tree. A unique volume at a certain position is represented by an object, a touchable (derived from *G4VTouchable*). It is created only if it is needed by the navigation system. To utilise importance sampling, importance values have to be assigned to volumes. The volumes have to be identified in a unique and durable way. In order to make use of the full replication mechanism in Geant4 it would be necessary to use touchable's. Use cases for importance sampling are typically based on simple geometries; therefore, the simple concept of geometry cells have been introduced with the class *G4GeometryCell* (see figure 4).

The class *G4GeometryCell* allows to define geometry cells for scoring and assignment of importance values. The geometry cells allow to identify a physical volume uniquely but only in a geometry using simple replicas. *G4GeometryCell* objects may easily be created e.g. during detector construction without using the navigation system. The simplification as well as the limitations of using geometry cells compared to touchables come from not taking hierarchical positions of physical volumes in the geometry tree into account.

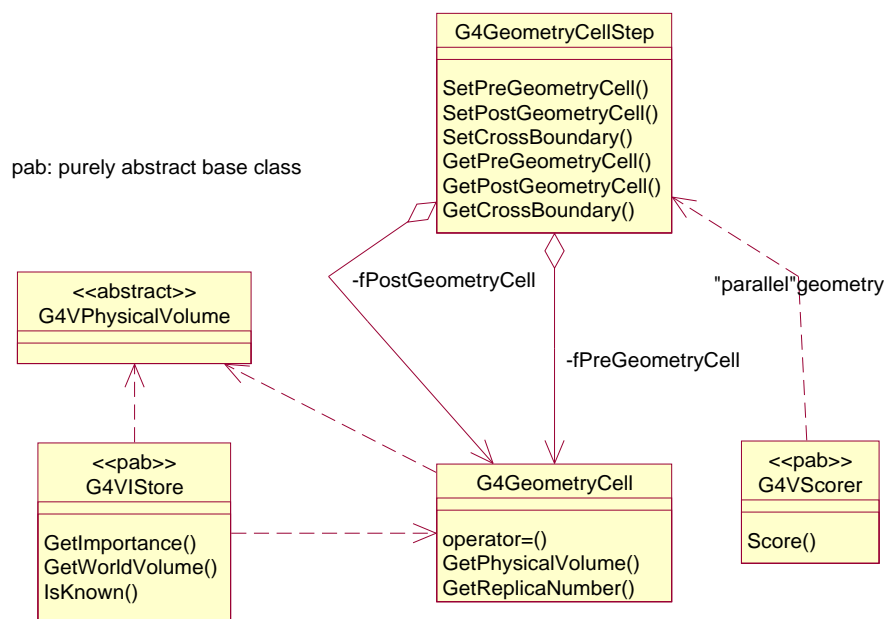


Figure 4: *G4GeometryCell* identifies a volume uniquely in simple geometries. *G4GeometryCellStep* holds two *G4GeometryCell* objects related to: the current cell and the last cell different from the current cell if the track already passed more than one cell. Also shown are the basic relations of *G4GeometryCell* and *G4GeometryCellStep* with other interfaces.

3.5 Importance value definition

A importance store separated from the usual geometry tree has been introduced for storing pairs of geometry cells and their associated importance values for the following reasons:

- No additional code is introduced in the geometry and therefore the performance of simulations not applying importance sampling or scoring are not affected.
- By creating multiple importance stores it is possible to apply different importance values a given cell for different particle types.

Importance stores must derive from the interface class *G4VStore* depicted in figure 5. The figure also shows relations of the class *G4VStore* to other parts of the implementation.

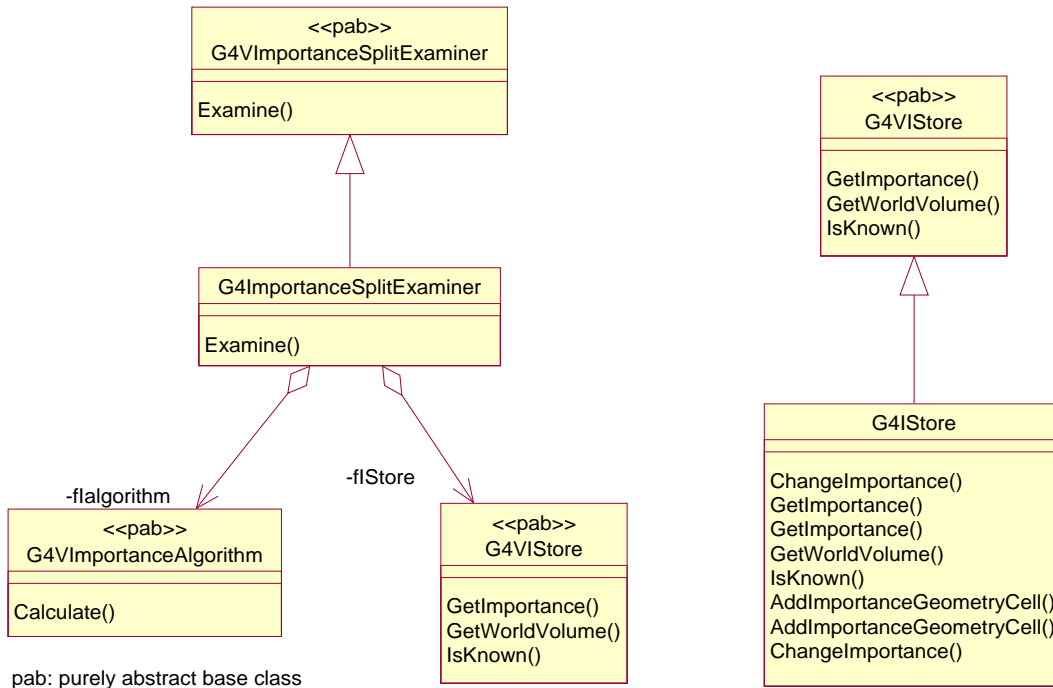


Figure 5: *G4VStore* defines the importance store interface. *G4IStore* is a concrete implementation. *G4IStore* allows to assign importance values to cells. *G4VImportanceSplitExaminer* defines the interface to obtain the number of particles and their weight when a track crosses the boundary between cells. The concrete implementation *G4ImportanceSplitExaminer* uses a *G4VStore* to obtain the cell importance values and a *G4VImportanceAlgorithm* to calculate the number of tracks and their weight.

3.6 Scoring

The basic service provided by scoring is defined by the interface class *G4VScorer*. The sampler classes introduced above configure the simulation with customised scorers derived from *G4VScorer* (see figure 6). A scorer uses a sampler responsible for a certain particle type. The scorer is messaged for every step of the concerned particles. Information is provided about the current *G4Step* and *G4GeometryCellStep*. The *G4GeometryCellStep* provides the information about two cells: the current cell and the last cell passed by the track. The two cells are different if the track has passed more than one cell already. A concrete implementation *G4Scorer* is provided. It produces scores similar to the controlling information in [11]. *G4Scorer* provides scores based on the following quantities:

- *D*: Step length between previous and post step point.
- *WD*: Weight of the particle at the previous step point times the step length.
- *WDT*: *WD* divided by the velocity of the particle at the previous step point.
- *WDE*: *WD*E*, weight times energy (both from previous step point) times step length.
- *WTE*: *WDE* divided by the velocity

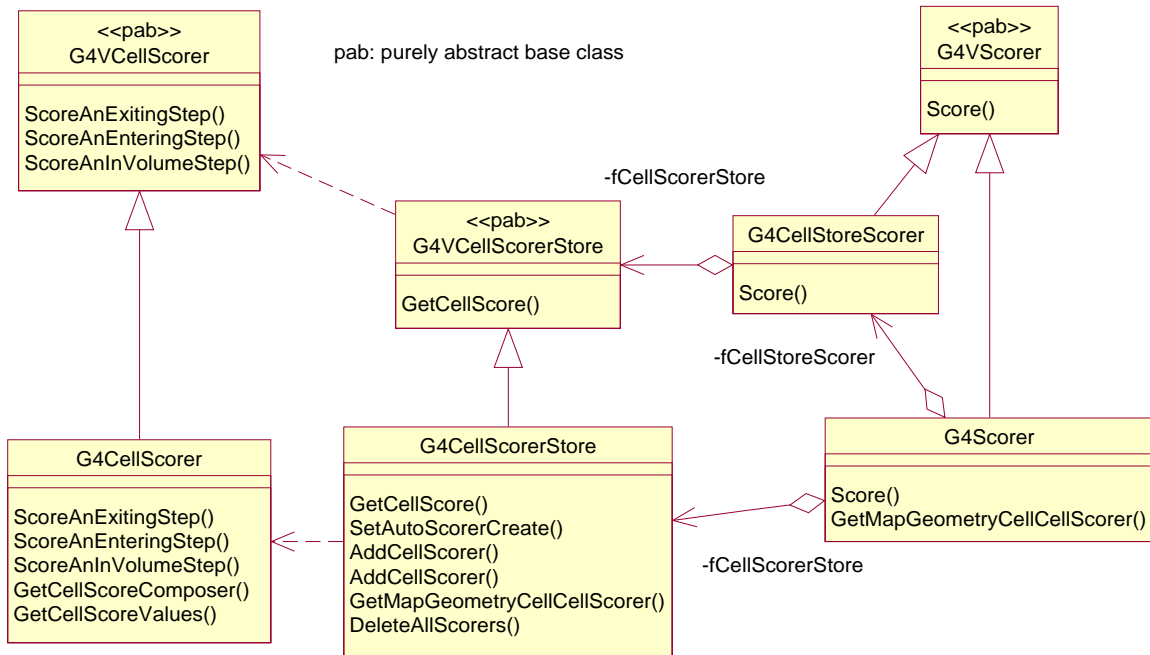


Figure 6: *G4VScorer* defines the scorer interface. *G4Scorer* is a concrete implementation providing cell wise scores represented by *G4CellScorer*. The concept of separating cell wise scores and the storing has been made explicit by the classes *G4VCellScorer* and *G4CellScorerStore*. The *G4CellStoreScorer* is responsible for messaging the cell-wise scorers via the *G4VCellScorer* interface.

The scores provided by *G4Scorer* are:

- "Importance": The importance of the cell.
- "Tr.Entering": The sum of tracks entering. Reentrant tracks are counted again.
- "Population": The number of tracks entering and created in a cell. Reentrant tracks are not counted again.
- "Collisions": Number of collisions. Steps ending at boundaries of the mass geometry are not counted, but collisions in other parallel geometries that might exist are currently counted, incorrectly, as collisions.
- "Coll*WGT": Weighted sum of collisions. The weight of the particle when it is just entering the collision, before any physics process took place at this point.
- "NumWGTedE": The number weighted energy: $\frac{\sum WTE}{\sum WDT}$
- "FluxWGTedE": The flux weighted energy: $\frac{\sum WDE}{\sum WD}$
- "Av.Tr.WGT": Average track weight: Importance $\times \frac{\sum WD}{\sum D}$

The implementation of the scorer provided with *G4Scorer* contains concepts which may be reused in customised scorers (see figure 6):

- The scoring is divided into cell scorers responsible for an individual geometry cell and a system responsible for messaging the cell scorers related to the cell a track is currently passing through.
- The messaging of cell scorers is done by *G4CellStoreScorer* implementing the interface *G4VScorer*. The cell scorers receive messages for scoring: a track entering the cell; a step within the cell; a track exiting the cell.
- The cell scorers may be stored by a cell scorer store derived from the interface class *G4VCellScorerStore*. *G4VCellScorerStore* stores may use the *G4CellStoreScorer*. *G4CellScorerStore* is a concrete implementation for *G4CellScorer* objects.
- Cell scorers implementing the interface *G4VCellScorer* receive messages from *G4CellStoreScorer*.

3.7 Outline of lower level concepts

The concepts described above are integrated into Geant4 by a layer of lower level services outlined in this section.

- Information about the tracking of particles needed by importance sampling and scoring is provided by the Geant4 tracking for classes derived from the kernel class *G4VProcess*. This system differentiates already by particle type and allows to change, add and remove tracks. It is therefore used for importance sampling and scoring.
- Transportation in a parallel geometry is implemented via a process (*G4ParallelTransport*). This process limits steps according to the parallel geometry. It retrieves geometry information and moves the track in the parallel geometry via the interface *G4VGeoDriver*. *G4ParallelNavigator* is a wrapper for the *G4Navigator* implementing the interface *G4VGeoDriver*.
- The creation of track copies are implemented by the same class used by both importance sampling processes for the mass and parallel geometry. The deletion of tracks is forwarded to the scoring process in case importance sampling and scoring are both used. This way the scoring process has the chance to score a track which should be deleted according to the Russian Roulette result.
- The information about cells is provided in the same way for mass or parallel geometries. Since no information about parallel geometries is available via the *G4Step* the *G4GeometryCellStep* objects are provided via a parallel stepper represented by the interface *G4VParallelStepper*. *G4ParallelTransport* updates the parallel stepper via the interface *G4VParallelStepper*. The importance sampling and the scoring processes obtain the *G4GeometryCellStep* objects via the *G4VParallelStepper*.
- The instantiation and connection between classes are done by the samplers (see section 3.3). The samplers use configurators according to the chosen configuration of importance sampling and scoring. The configurators implementing the interface *G4VSamplerConfigurator* instantiate and connect objects of the lower level classes outlined in this section.

4 Verification

In this section a simulation of the TIARA benchmark experiment [9] is used to verify that: Geant4’s geometrical importance sampling, described above, reduces computing time and leaves the mean value of physical quantities unchanged. In the TIARA experiment neutron fluxes are measured behind several concrete shields of different thicknesses bombarded by neutrons with energy distributions peaking at 40 MeV and 65 MeV. The neutron flux is measured on and off the beam axis.

4.1 Brief description of the experiment

Neutrons are produced by two proton beams of 43 MeV and 68 MeV energy bombarded on an ${}^7\text{Li}$ -target. The neutron energy spectra produced by the two different proton beams are reproduced in figure 7.

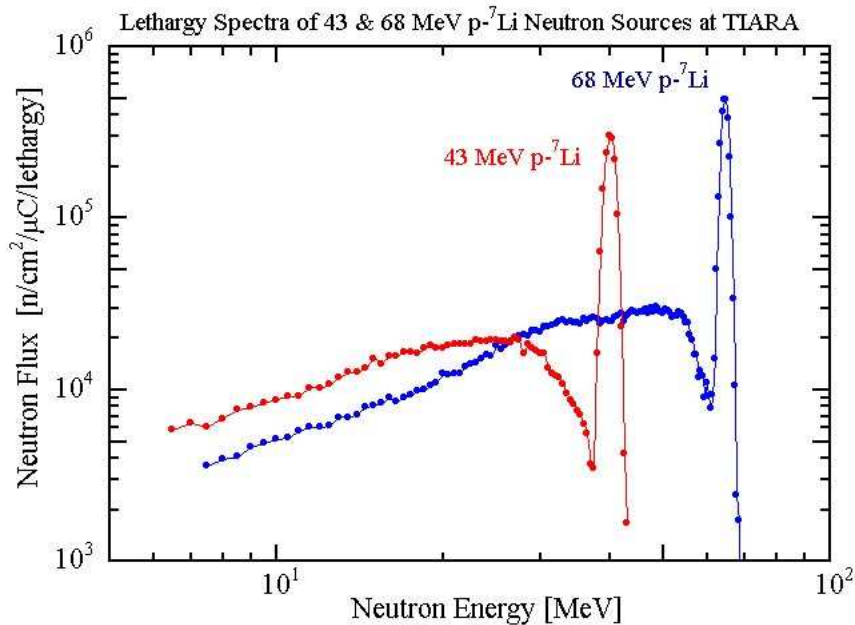


Figure 7: “Lethargy spectra of 43 & 68 p - ${}^7\text{Li}$ neutron sources at TIARA” taken from [12]

The neutron beam is directed onto concrete shields composed out of 25 *cm* thick concrete layers. For the 43 *MeV* p - ${}^7\text{Li}$ neutrons shields of 25, 50, 100 and 150 *cm* thickness are used. In case of the 68 *MeV* proton beam the additional concrete shield of thickness 200 *cm* is used. A cross section sketch of the experimental setup is reproduced in figure 8. For the shields of thickness 25 and 50 *cm* additional collimators of thicknesses 40 and 80 *cm* are used in the 43 and 68 *MeV* proton beam cases respectively.

Energy dependent neutron fluxes obtained with a BC501A scintillator detector and a bonner ball detector are shown in [9]. The scintillator detector was used on the beam line for all the shields. For the 25 and 50 *cm* thick shields the scintillator was also used 20 and 40 *cm* off the beam line.

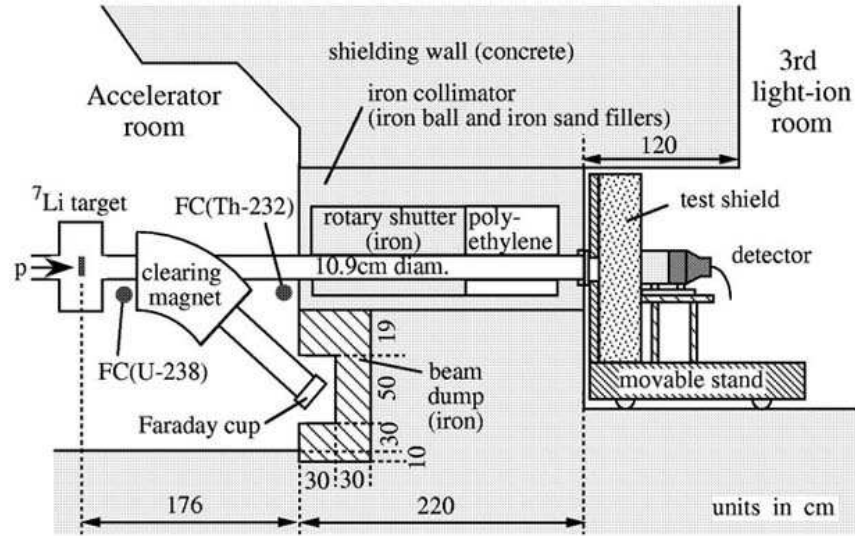


Figure 8: “Cross sectional view of TIARA neutron beam course” taken from [12]

4.2 Geant4 simulation of the TIARA experiment

The geometry used for the simulation

Figure 9 shows a side view and a view from the back of the mass geometry used in the simulation.

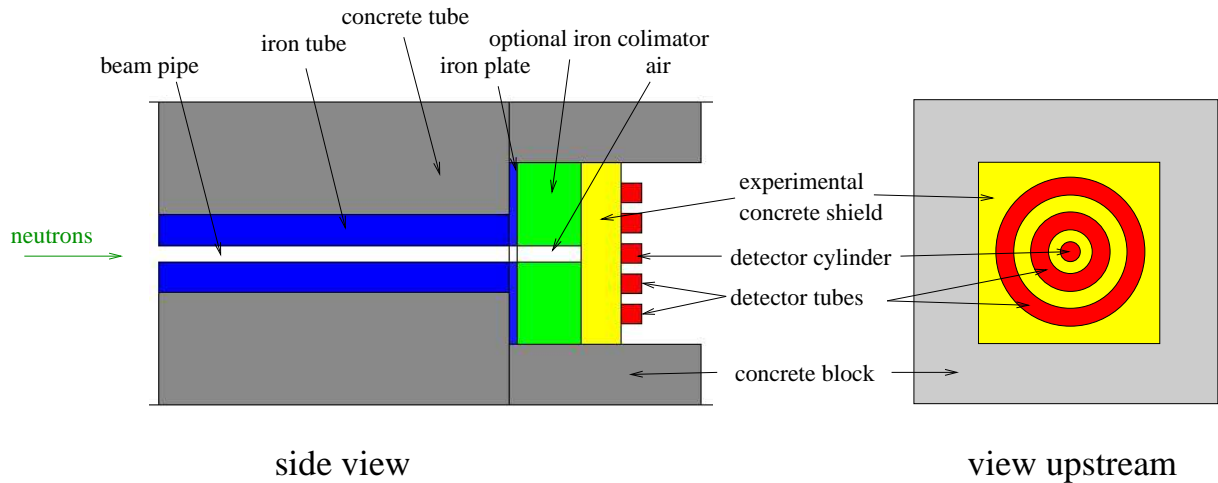


Figure 9: The simulation geometry viewed from the side and from the back. The right figure clarifies the tube shape of the detectors used for the simulation.

Upstream of the neutron beam, figure 9, the 10.9 cm diameter beam pipe is surrounded by a 52 cm diameter iron tube surrounded by a 200 cm diameter concrete tube. The box shaped experimental concrete shields are located downstream, right in the side view. Between the exit of the beam pipe and the experimental concrete shields a 5 cm thick iron plate and,

optionally, an additional 40 or 80 *cm* thick iron collimator are placed. On the beam line the iron plate and collimator have holes of the beam pipe radius filled with air. The iron shield, collimator and the experimental concrete shield have lateral dimensions of 120 *cm*. The concrete wall on the right side is modelled by concrete blocks of dimensions: 120 *cm* along the beam axis and 40 *cm* in radial direction, surrounding the experimental setup. On the right of the experimental concrete shield are the detector volumes.

This geometry is similar to a geometry used in simulations in [9]. The concrete is composed according to the published values. Details of the volumes used for flux estimation on the right of the experimental shields are given below.

The physical quantities to be calculated

The verification of importance sampling is done by a Geant4 calculation for the fluxes [12] obtained with the BC501A scintillator. The BC501A scintillator is sensitive for neutrons with energies above a few *MeV*. The results of the BC501A scintillator are estimated in the calculation by a track length estimator for the flux. On the beam axis the estimation is done using a cylindrical volume of 12.9 *cm* diameter and height. The fluxes off axis are estimated with 12.9 *cm* thick tubes of middle radii 20 and 40 *cm*, for the off axis measurements respectively, centred on axis (see figure 9). The length of the tubes along the beam axis are 12.9 *cm*. The experimental setup is not cylinder symmetric but it has the symmetries of a square. By using tubes for estimating the fluxes off axis the chances for tracks being scored is clearly increased compared to using the same detector as used on axis. The difference between square and cylinder symmetry effects only tracks scattering from some small regions 60 *cm* off the beam axis back towards the detectors. For test purposes a simulation using a square shaped geometry with the same cylindrical detector used off beam axis as on beam axis was done. The estimated flux using a tube shaped detector compared to the estimated flux using the test geometry of the detector were found to be equal within the errors.

In the simulation the detector volumes are evacuated. The flux is estimated as:

$$f_{\text{est.}} = \sum_{\text{neutron tracks}} wl/V_D \quad (2)$$

the sum over the neutron track length *l* multiplied by the particle weight *w* in the detector volume V_D divided by the volume V_D . The flux is measured separately for bins of energy given in [12]. The results from the simulation are scaled for comparison with the experimental data. In [9] values for the neutron flux F_{src} in $[\frac{n}{cm^2\mu C}]$, 401 *cm* distant from the target, in the peak of the neutron energy spectra are given per one μC of proton beam charge. In the given source neutron energy spectrum the flux in the peak region is normalised to one.

The flux F_{det} measured by the experiment is compared with the flux f_{est} per cm^2 estimated in the volumes described above multiplied with the scaling factor *S*:

$$S = \frac{F_{src}}{f_{gen}} = \frac{A_b F_{src}}{N_{gen,peak}},$$

where f_{gen} is the generated flux in the peak region 401 *cm* distant from the target through the beam cross section of $A_b = 93.31cm^2$. $N_{gen,peak}$ is the number of neutrons generated with energies in the peak region.

The neutron source

For the simulation neutrons are sampled according to the energy spectra figure 7. The

generated neutron directions are limited to a small cone covering the beam pipe cross section area at 401 *cm* distant from the target position. This way outer most neutrons hit the additional iron collimators used in the experiments with 25 and 50 *cm* thick shields. The directions of the neutrons, in the cone, are distributed isotropically.

The physics description

In Geant4 the physics description is provided via so called physics lists. For the hadronic physics description the framework [13] is used. In this simulation a modified version of the physics list LHEP_BIC and Packaging library 2.1 [14] (currently to be found under “low energy nucleon penetration shielding”, “For geant4 5.0, and patches” on the web site: Educated Guess Physics Lists for Geant4 Hadronic Physics <http://cmsdoc.cern.ch/~hpw/GHAD/HomePage/index.html>) implementing a intra nuclear binary cascade model is used. The modified physics list uses tabulated data for neutron energies below 20 *MeV* and the binary cascade model for neutron energies above 20 *MeV*. Other particles simulated are: photon, proton, deuteron, triton and alpha. Since the scintillator is sensitive only above a few *MeV* and no fissionable material is involved cuts on particle energies have been introduced. Table 10 lists the particles and the cuts applied to them.

particle	cut in [<i>MeV</i>]
neutron	3
photon	1
proton	1
deuteron	1
triton	1
alpha	1

Figure 10: *The particles and energy cuts used in the simulation.*

4.3 The setup for the geometrical importance sampling

For the shields of thicknesses 25 and 50 *cm* the gain in computing time achievable by importance sampling is much smaller than for the thicker shields. Therefore in this note importance sampling is only applied in cases of experimental shield thicknesses: 100 *cm*, 150 *cm* and 200 *cm*. As in [9] the 200 *cm* thick shield is only used for the 68 *MeV* proton energy case.

Importance geometry

The importance geometry is constructed using a parallel geometry slightly overlapping the mass geometry. It basically follows the design of figure 1 section 2.1. The world volume of the parallel geometry is a box covering the world volume of the mass geometry. Box shaped slabs with the same dimensions as the parallel world volume perpendicular to the beam axis and varying dimension along the beam axis are placed in the region of the experimental concrete shields. These slabs are the cells most important for geometrical importance sampling. Another slab filling the remaining area of the parallel geometry is placed to the right of these slabs. Table 1 lists the dimensions along the beam axis of the boxes in the region of the concrete shields for the different energies and shield widths used.

Importance values

The parallel world volume and the first slab in the region of the experimental concrete shield are assigned an importance of 1. This way particles are not split when entering the concrete shield from the source direction. The importance value of the remaining slabs are determined by doubling the value of the slab to the left. An exception is the last slab filling up the region behind the experimental shield, which has the same importance value as the last slab in the

Energy [MeV]	shield width [cm]	length [cm] of cells
43	100	6×15 cm and 1×10 cm
	150	10×15 cm
68	100	5×20 cm
	150	6×20 cm and 2×15 cm
	200	10×20 cm

Table 1: *Dimensions along the beam axis of the importance cells in the region of the experimental concrete shields.*

shield region. Therefore, particles exiting the concrete shield into the detector region are not split.

4.4 Results and FOM comparison for analog and non-analog calculations

The experimental neutron flux data taken from [9] are compared to the values obtained with Geant4. Two neutron energy regions for each source spectrum are used for quantitative comparison. The first regions are below the peak: 10-35 MeV for 43 MeV p-⁷Li neutrons, 10-60 MeV for 68 MeV p-⁷Li neutrons; the second regions are the peak regions: 35-45 MeV for 43 MeV p-⁷Li neutrons, 60-70 MeV for 68 MeV p-⁷Li neutrons. The above boundaries are also used in [9]. In the two neutron energy regions FOM_{imp.} and FOM_{ana.} have been calculated for Geant4 simulations applying and not applying importance sampling respectively. The gain in computing time by using importance sampling compared to the analog calculation is estimated by G :

$$G = \frac{\text{FOM}_{\text{imp.}}}{\text{FOM}_{\text{ana.}}} \quad (3)$$

If the statistics is adequate G can be interpreted as an estimate of the factor of time the analog calculation would have to run longer than the non-analog calculation to achieve the same precision measured by the variance.

Neutron fluxes on the beam axis are shown in the tables 2 and 3. The fluxes obtained 20 and 40 cm off beam axis are shown in the tables 4 and 5. The neutron fluxes are integrated in the two regions mentioned above. The values are compared to the experimental data and the ratio of simulated to experimental flux is given. Additionally the values from calculations given in [9] are shown. For the shields with thicknesses above 50 cm the gains G , equation 3, of FOM values are shown (see tables 2 and 3).

The largest gains, $G = 89$ (see table 3) and $G = 81$ (see table 2), are achieved in the neutron energy region below the peak for the 200 cm shield with the 68 MeV p-⁷Li neutrons and the 150 cm shield with the 43 MeV p-⁷Li neutrons respectively.

The gains G obviously show a strong dependence on the shield width. G is, for example, for the 68 MeV p-⁷Li neutrons, for the 150 cm concrete shield, only about a fifth of G for the 200 cm shield (see table 3). G is also strongly dependent on the neutron energies. For example for the 150 cm thick shield where G for the 68 MeV p-⁷Li neutrons is less than a

Shield Width	Exp. or a Sim.	10 - 35 MeV				35 - 45 MeV			
		Flux [$\frac{n}{cm^2\mu C}$]	R [%]	$\frac{Sim.}{Exp.}$	G	Flux [$\frac{n}{cm^2\mu C}$]	R [%]	$\frac{Sim.}{Exp.}$	G
25 cm	Exp	1.87E+03	–	–		2.69E+03	–	–	
	MORSE	2.08E+03	–	1.11		2.89E+03	–	1.07	
	G4-ana	1.61E+03	0.68	0.86		2.99E+03	0.50	1.11	
50 cm	Exp	1.56E+02	–	–		3.10E+02	–	–	
	MORSE	2.23E+02	–	1.42		3.26E+02	–	1.09	
	G4-ana	1.81E+02	1.26	1.16		5.36E+02	0.75	1.79	
100 cm	Exp	3.34E+00	–	–		5.04E+00	–	–	
	MORSE	5.67E+00	–	1.70		6.01E+00	–	1.19	
	G4-imp	5.73E+00	1.92	1.72	11	1.68E+01	1.52	3.33	7.3
	G4-ana	6.13E+00	6.41	1.84		1.57E+01	4.10	3.12	
150 cm	Exp	1.10E-01	–	–		1.22E-01	–	–	
	MORSE	2.31E-01	–	2.11		1.54E-01	–	1.26	
	G4-imp	2.57E-01	1.40	2.34	81	5.46E-01	1.24	4.48	55
	G4-ana	2.50E-01	6.32	2.27		5.10E-01	4.59	4.18	

Table 2: Transmitted neutron fluxes on the beam axis for 43 MeV $p\text{-}^7\text{Li}$ neutrons. The experimental data and the MORSE calculations are taken from [9]. For all shield thicknesses the analog Geant4 calculations (G4-ana) are shown. The values (G4-imp) obtained using Geant4 with importance sampling are shown for shields thicker than 50 cm. The ratios of the simulated to the experimental fluxes are given in the columns $\frac{Sim.}{Exp.}$ and the relative statistical errors in the columns R. The columns G list the estimated gains in computing time by using importance sampling.

quarter of that for the 43 MeV $p\text{-}^7\text{Li}$ neutrons (see tables 3 and 2). This dependency is also obvious since the cross sections for neutron elastic scattering and the deflection in elastic scattering increase with decreasing neutron energies.

These results suggest that even higher efficiencies can be expected for neutrons with lower energies for comparable shield widths.

The figures 11, 12, 13 and 14 compare neutron fluxes on and 20 and 40 cm off axis for the 25 and 50 cm thick shields. Importance sampling was not found to be useful for these calculations. Nevertheless, the results are given for completeness.

The figures 15, 16 and 17 show the neutron flux distributions on beam axis for the concrete shields 100 cm and thicker for the 43 and 68 MeV $p\text{-}^7\text{Li}$ neutrons respectively. The figures compare the results of the analog simulations with the results obtained using geometrical importance sampling. The comparison shows that the analog and non-analog calculations agree very well within the errors. In most cases the errors obtained using importance sampling are clearly much smaller than the errors obtained in the non-analog calculations. The only exception to the above is the comparison for the 68 MeV $p\text{-}^7\text{Li}$ neutrons on a 100 cm shield where the errors in both calculations are about equal. In this

43 MeV p->Li
on concrete(25 cm thick)

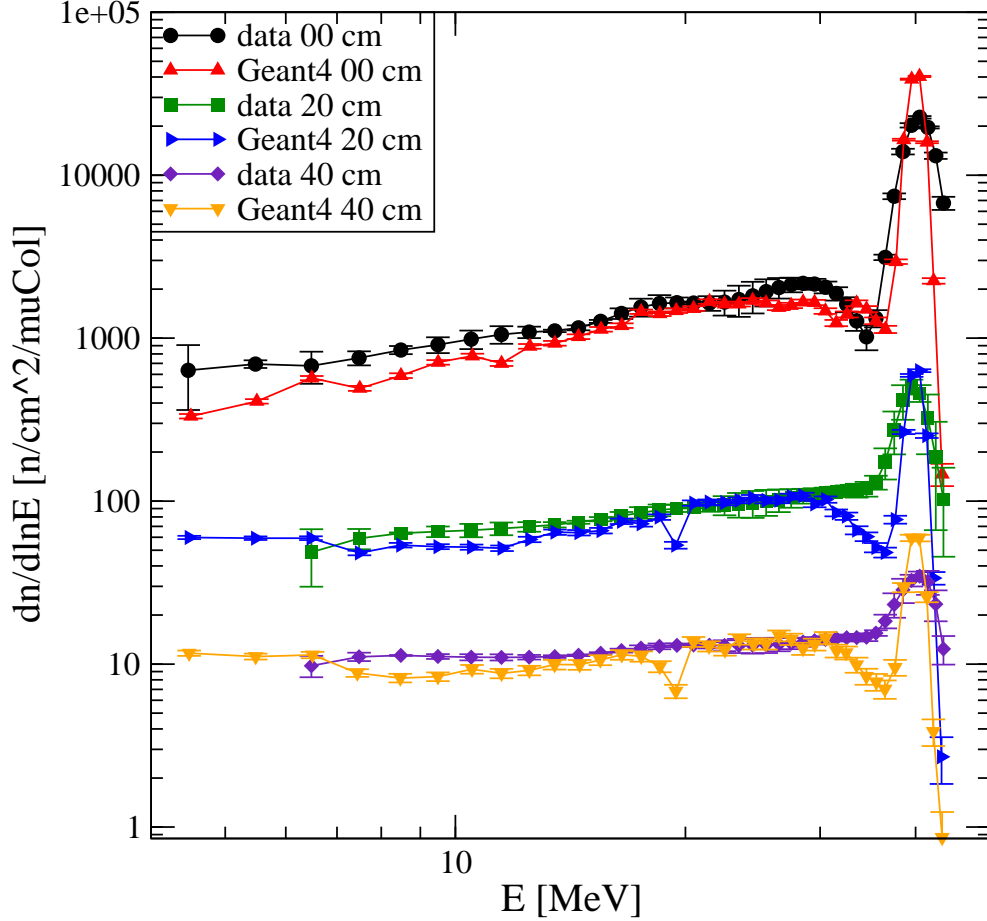


Figure 11: Neutron energy spectra through 25 cm of concrete shield on and 20 and 40 cm off the beam axis for the 43 MeV $p\text{-}^7\text{Li}$ neutrons. The data points are from [9].

case the computing time of the analog calculation was four times longer than the computing time for the importance sampled calculation (see table 6) and the gain in computing time is estimated to be about 4 too (see table 3). Therefore, the close agreement of the errors for the analog and non-analog calculation is expected and supports the method of estimating the gain in computing time.

The running time of the simulations with and without importance sampling has been equal for the 43 MeV $p\text{-}^7\text{Li}$ neutrons with the 100 cm concrete shield and for the 68 MeV $p\text{-}^7\text{Li}$ neutrons with the 150 cm concrete shields (see table 6). Whereas for the 43 MeV $p\text{-}^7\text{Li}$ neutrons with the 150 cm shield and the 68 MeV $p\text{-}^7\text{Li}$ neutrons with the 200 cm shield the running time for the non-analog simulation is only a quarter of the running time for the analog calculation. These results, significant smaller errors even with much shorter computing time, demonstrates again the expected gain in efficiency from geometrical importance sampling.

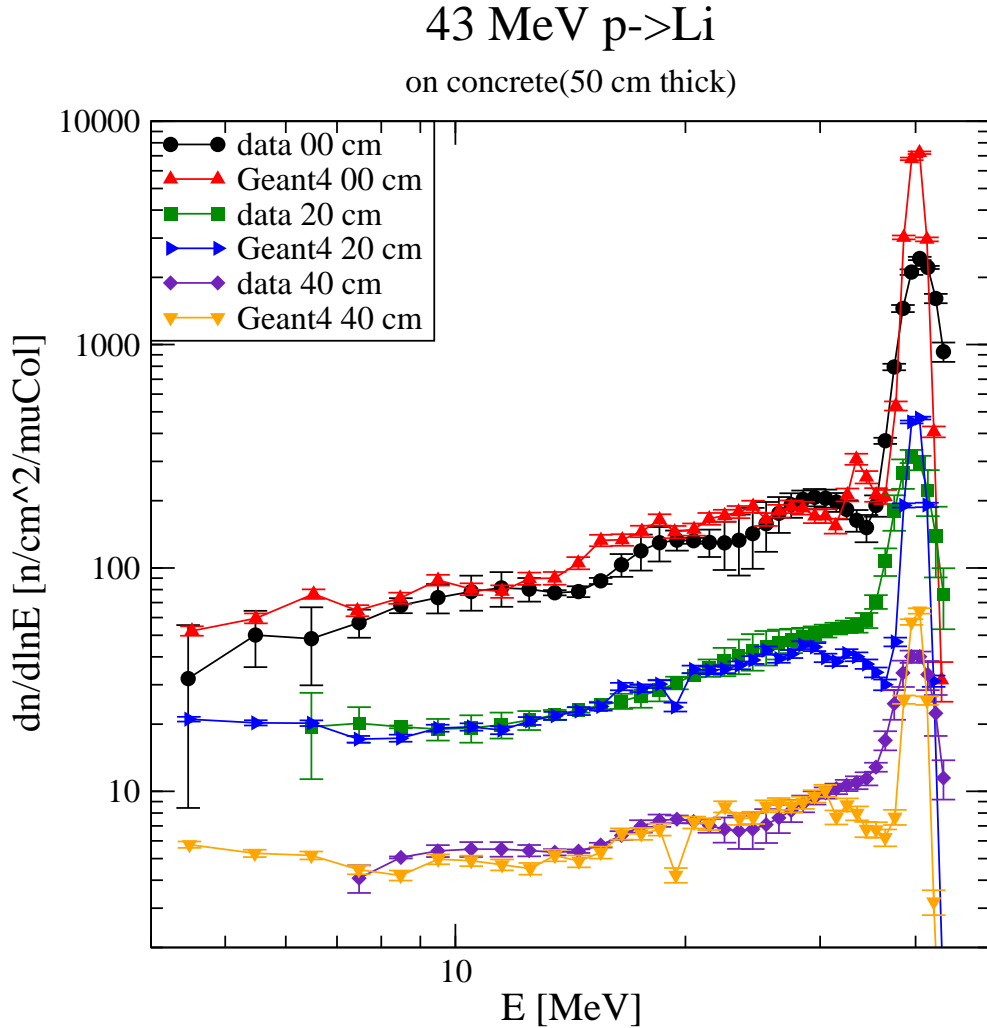


Figure 12: Neutron energy spectra through 50 cm of concrete shield on and 20 and 40 cm off the beam axis for the 43 MeV $p\text{-}^7\text{Li}$ neutrons. The data points are from [9].

For the calculations two basically identical computers: pcgeant2 and pcgeant3 have been used. Both computers have two processors: Intel(R) Xeon(TM) CPU 1700MHz and run a GNU/Linux version CERN RedHat 7.3. The gcc compiler version 3.2 was used. The processing times and the computers used for the different calculations are listed in table 6.

Taking the computing times from table 6 and the relative statistical errors from tables 2 and 3 the values for G may be reproduced using formula 3. Note that the values of G calculated this way will slightly differ from the listed values due to the rounding applied to the listed relative errors.

4.5 Discussion of the results

The values $\frac{Sim.}{Exp.}$ comparing the Geant4 results to the experimental data lie mostly well between 0.5 and 2 for the 68 MeV $p\text{-}^7\text{Li}$ neutrons (see table 3). In contrast large deviations

68 MeV p->Li
on concrete(25 cm thick)

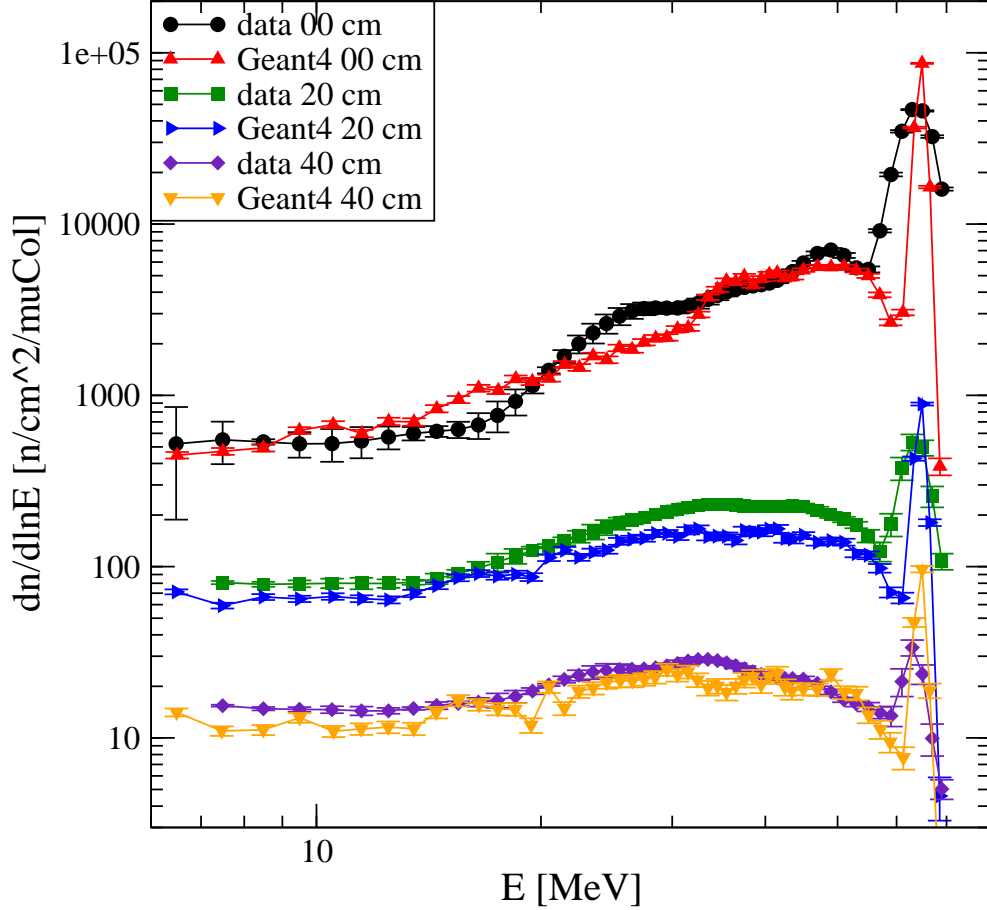


Figure 13: Neutron energy spectra through 25 cm of concrete shield on and 20 and 40 cm off the beam axis for the 68 MeV $p\text{-}^7\text{Li}$ neutrons. The data points are from [9].

up to $\frac{Sim.}{Exp.} = 4.48$ are found for the 43 MeV $p\text{-}^7\text{Li}$ neutrons (see table 2).

The distributions figures 15, 16, 17 obtained with the analog and non-analog Geant4 simulations agree very well within the errors. This confirms one of the main goals of this note: applying geometrical importance sampling does not change the estimated mean values of the observables. This holds even for the encountered case of deviations of the simulations from the experimental data.

Two reasons have to be kept in mind to understand these deviations: The errors of the experimental data have to be considered and the physics description of Geant4 in the energy region above 20 MeV and below energies of order 100 MeV is still under development. The physics model used for this energy region, the intra nuclear binary cascade, is designed for energies in the 100 MeV region and above. The energy region below 20 MeV is well covered with tabulated cross section and angular distribution data and is therefore expected to be fairly accurate. This means, that especially for the neutrons with low energies but above

68 MeV p->Li
on concrete(50 cm thick)

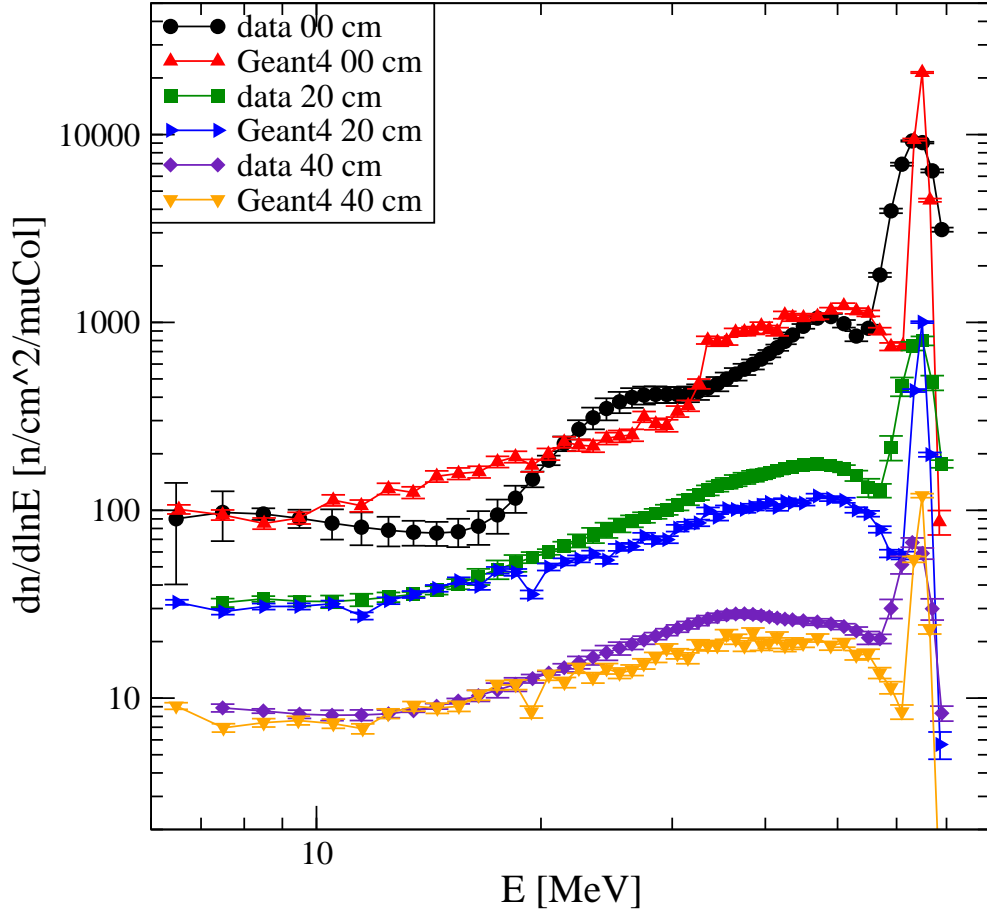


Figure 14: Neutron energy spectra through 50 cm of concrete shield on and 20 and 40 cm off the beam axis for the 68 MeV $p\text{-}^7\text{Li}$ neutrons. The data points are from [9].

20 MeV deviations are expected to be large. This may explain the difference in deviations for the 43 and 68 $p\text{-}^7\text{Li}$ neutrons. The cross-sections in the region above 20 MeV to about 100 MeV are not known with the same accuracy as below 20 MeV. For a more accurate simulation the cross-sections would have to be tuned. The scaling would have to be applied within the errors of the cross-section measurements.

Another potential reason is the effect of detector resolution which has not been taken into account by the Geant4 simulations. The next section shows that deviations of the fluxes integrated in the two energy regions below and in the peak region, presented in the tables of this section, from the experimental data can not be explained by the missing detector resolution in the simulation.

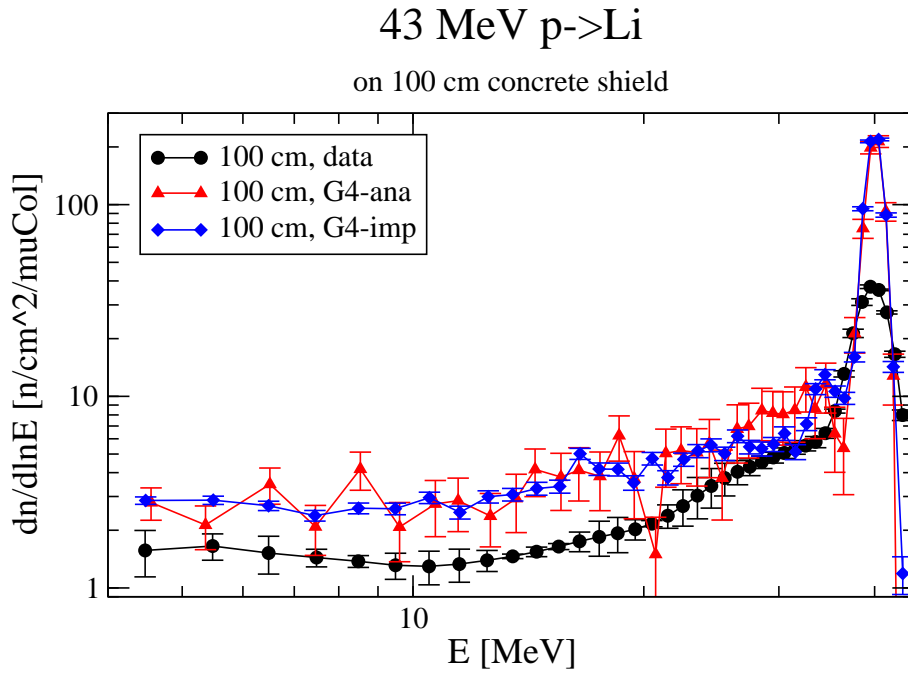


Figure 15: Transmitted neutron flux through 100 cm of concrete shield on the beam axis for 43 MeV $p^{-7}\text{Li}$ neutrons. Two distributions obtained with Geant4: “G4-imp” with importance sampling and “G4-ana” analog, are shown.

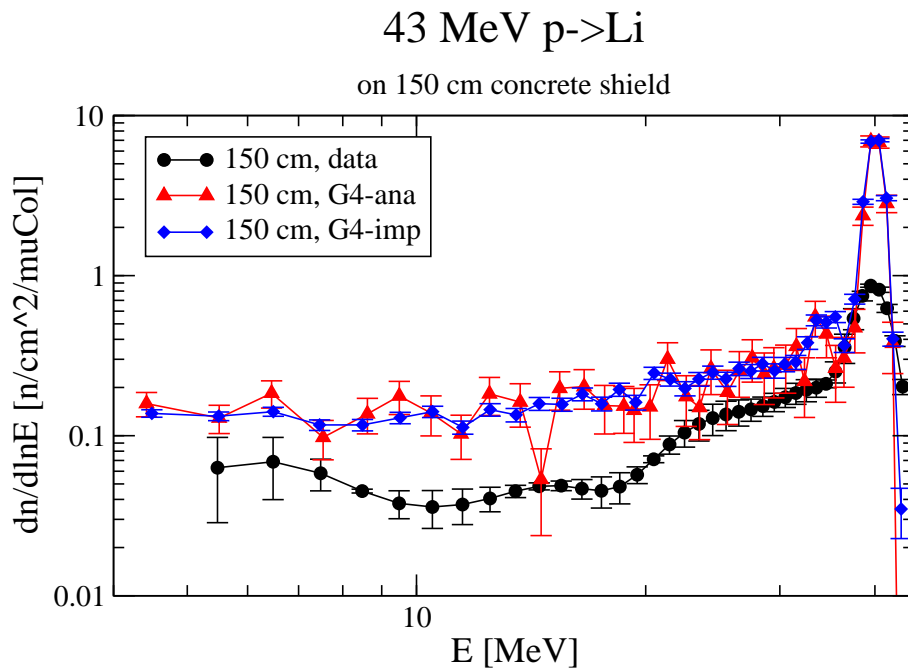


Figure 16: Transmitted neutron flux through 150 cm of concrete shield on the beam axis for 43 MeV $p^{-7}\text{Li}$ neutrons. Two distributions obtained with Geant4: “G4-imp” with importance sampling and “G4-ana” analog, are shown.

Shield Width	Exp. or a Sim.	10 - 60 MeV				60 - 70 MeV			
		Flux [$\frac{n}{cm^2\mu C}$]	R [%]	$\frac{Sim.}{Exp.}$	G	Flux [$\frac{n}{cm^2\mu C}$]	R [%]	$\frac{Sim.}{Exp.}$	G
25 cm	Exp	5.52E+03	–	–		5.46E+03	–	–	
	MORSE	5.82E+03	–	1.05		5.93E+03	–	1.09	
	G4-ana	4.43E+03	0.54	0.80		4.43E+03	0.55	0.81	
50 cm	Exp	8.40E+02*	–	–		1.08E+03	–	–	
	MORSE	9.14E+02	–	1.09		1.19E+03	–	1.10	
	G4-ana	8.25E+02	0.79	0.98		1.12E+03	0.69	1.04	
100 cm	Exp	4.27E+01	–	–		4.81E+01	–	–	
	MORSE	5.06E+01	–	1.19		4.79E+01	–	0.99	
	G4-imp	5.38E+01	0.55	1.26	4.1	7.83E+01	0.54	1.63	3.1
	G4-ana	5.47E+01	0.56	1.28		7.85E+01	0.48	1.63	
150 cm	Exp	3.08E+00	–	–		2.20E+00	–	–	
	MORSE	3.81E+00	–	1.24		2.20E+00	–	0.88	
	G4-imp	3.76E+00	1.19	1.22	21	4.52E+00	1.38	2.05	13
	G4-ana	3.73E+00	5.42	1.21		4.81E+00	4.91	2.18	
200 cm	Exp	5.17E-01	–	–		2.80E-01	–	–	
	MORSE	4.43E-01	–	0.86		2.80E-01	–	0.79	
	G4-imp	3.41E-01	1.33	0.66	89	2.71E-01	1.81	0.97	59
	G4-ana	3.37E-01	6.26	0.65		2.86E-01	6.92	1.02	

Table 3: Transmitted neutron fluxes on the beam axis for 68 MeV $p^{-7}Li$ neutrons. The experimental data and the MORSE calculations are taken from [9]. For all shield thicknesses the analog Geant4 calculations (G4-ana) are shown. The values (G4-imp) obtained using Geant4 with importance sampling are shown for shields thicker than 50 cm. The ratios of the simulated to the experimental fluxes are given in the columns $\frac{Sim.}{Exp.}$ and the relative statistical errors in the columns R. The columns G list the estimated gains in computing time by using importance sampling.

Shield Width	distance off axis	Exp. or a Sim.	10 - 35 MeV			35 - 45 MeV		
			Flux [$\frac{n}{cm^2\mu C}$]	R [%]	$\frac{Sim.}{Exp.}$	Flux [$\frac{n}{cm^2\mu C}$]	R [%]	$\frac{Sim.}{Exp.}$
25 cm	20 cm	Exp	1.10E+02	–	–	6.52E+01	–	–
		MORSE	1.37E+02	–	1.25	6.41E+01	–	0.98
		G4-ana	9.66E+01	0.82	0.87	4.92E+01	1.12	0.75
	40 cm	Exp	1.57E+01	–	–	5.58E+00	–	–
		MORSE	1.61E+01	–	1.03	6.54E+00	–	1.17
		G4-ana	1.39E+01	1.54	0.89	5.14E+00	2.48	0.92
50 cm	20 cm	Exp	4.17E+01	–	–	4.23E+01	–	–
		MORSE	5.58E+01	–	1.33	5.00E+01	–	1.18
		G4-ana	3.80E+01	0.82	0.91	3.63E+01	0.82	0.86
	40 cm	Exp	8.82E+00	–	–	5.96E+00	–	–
		MORSE	1.23E+01	–	1.39	5.79E+00	–	0.97
		G4-ana	8.23E+00	1.25	0.93	4.97E+00	1.56	0.83

Table 4: Transmitted neutron fluxes 20 and 40 cm off the beam axis for 43 MeV $p\text{-}^7\text{Li}$ neutrons. The experimental data and the MORSE calculations are taken from [9]. The values in columns G4-ana are calculated without importance sampling. The ratios of the simulated to the experimental fluxes are given in the columns $\frac{Sim.}{Exp.}$ and the relative statistical errors in the columns R.

Shield Width	distance off axis	Exp. or a Sim.	10 - 60 MeV			60 - 70 MeV		
			Flux [$\frac{n}{cm^2\mu C}$]	R [%]	$\frac{Sim.}{Exp.}$	Flux [$\frac{n}{cm^2\mu C}$]	R [%]	$\frac{Sim.}{Exp.}$
25 cm	20 cm	Exp	2.76E+02	–	–	5.53E+01	–	–
		MORSE	3.00E+02	–	1.12	4.67E+01	–	0.84
		G4-ana	2.05E+02	0.73	0.74	4.87E+01	1.49	0.88
	40 cm	Exp	3.58E+01	–	–	2.94E+00	–	–
		MORSE	4.26E+01	–	1.19	1.53E+00	–	0.52
		G4-ana	3.07E+01	1.36	0.86	5.31E+00	3.21	1.8
50 cm	20 cm	Exp	1.65E+02	–	–	8.27E+01	–	–
		MORSE	2.26E+02	–	1.36	7.27E+01	–	0.88
		G4-ana	1.19E+02	0.61	0.72	5.26E+01	0.90	0.68
	40 cm	Exp	3.14E+01	–	–	6.77E+00	–	–
		MORSE	3.92E+01	–	1.24	5.89E+00	–	0.87
		G4-ana	2.49E+01	0.94	0.79	6.41E+00	1.82	0.95

Table 5: Transmitted neutron fluxes 20 and 40 cm off the beam axis for 68 MeV $p\text{-}^7\text{Li}$ neutrons. The experimental data and the MORSE calculations are taken from [9]. The values in columns G4-ana are calculated without importance sampling. The ratios of the simulated to the experimental fluxes are given in the columns $\frac{Sim.}{Exp.}$ and the relative statistical errors in the columns R.

shield width [cm]	43 MeV $p\text{-}^7\text{Li}$		68 MeV $p\text{-}^7\text{Li}$	
	time [hour]	system	time [hour]	system
25	3	pcgeant2	3	pcgeant3
50	10	pcgeant2	10	pcgeant3
100	12	pcgeant2	300	pcgeant3
100 imp.	12	pcgeant2	75	pcgeant3
150	288	pcgeant3	50	pcgeant3
150 imp.	72	pcgeant3	50	pcgeant3
200	–	–	400	pcgeant2
200 imp.	–	–	100	pcgeant2

Table 6: List of processing times and computers used for the different calculations. The rows marked with “imp.” refer to the importance sampled calculations. The columns “system” show which computers have been used.

68 MeV p->Li

on 100, 150, 200 cm concrete shield

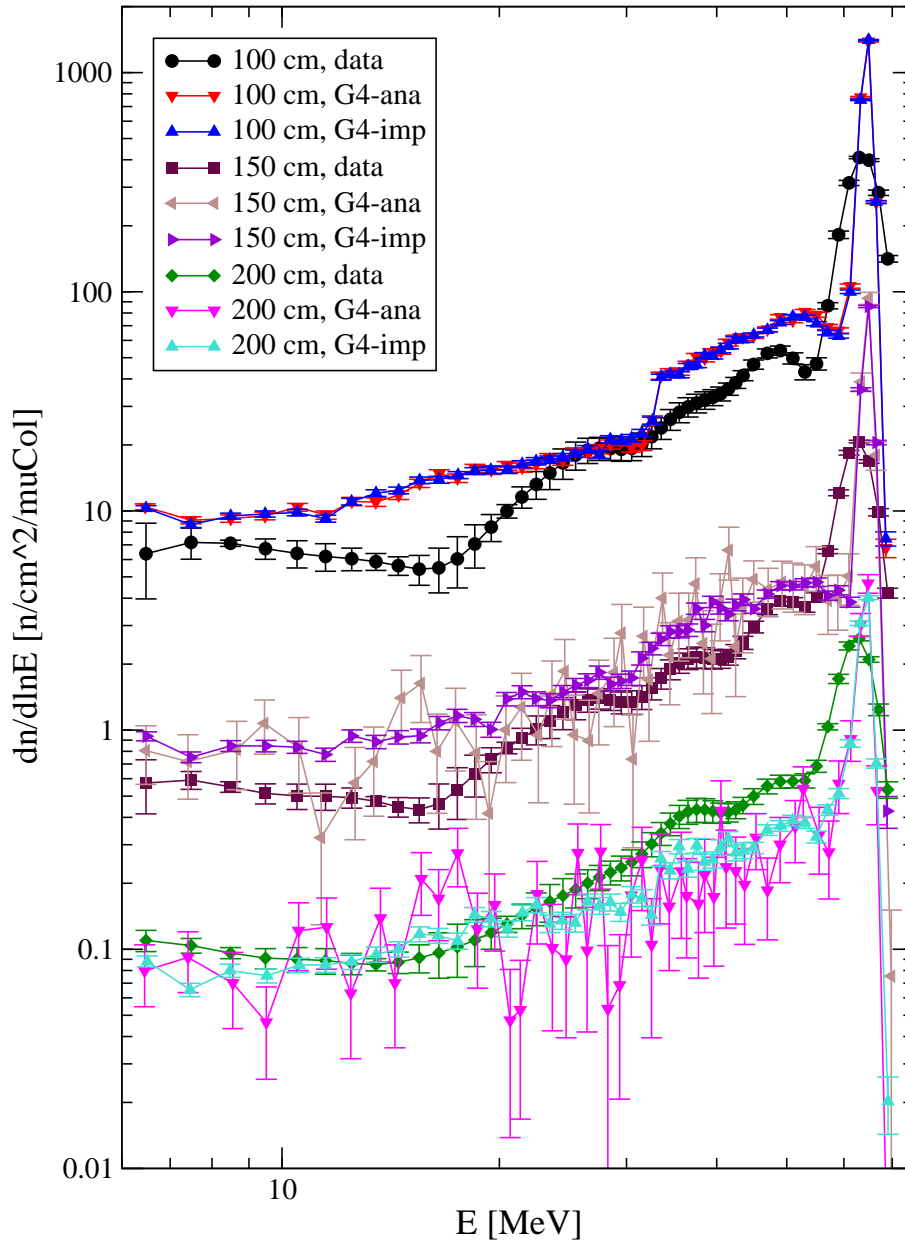


Figure 17: Transmitted neutron flux through 100, 150 and 200 cm of concrete shields on the beam axis for 68 MeV $p\text{-}^7\text{Li}$ neutrons. The experimental data are taken from [9]. Two distributions obtained with Geant4: “G4-imp” with importance sampling and “G4-ana” analog, are shown for every shield.

4.6 Effect of detector resolution

The effect of a finite detector resolution has been checked by smearing neutron energies. Figure 18 and table 7 oppose the fluxes obtained with and without smearing for the 43 MeV proton source and the 100 cm thick concrete shield. Only for this check the neutron energies

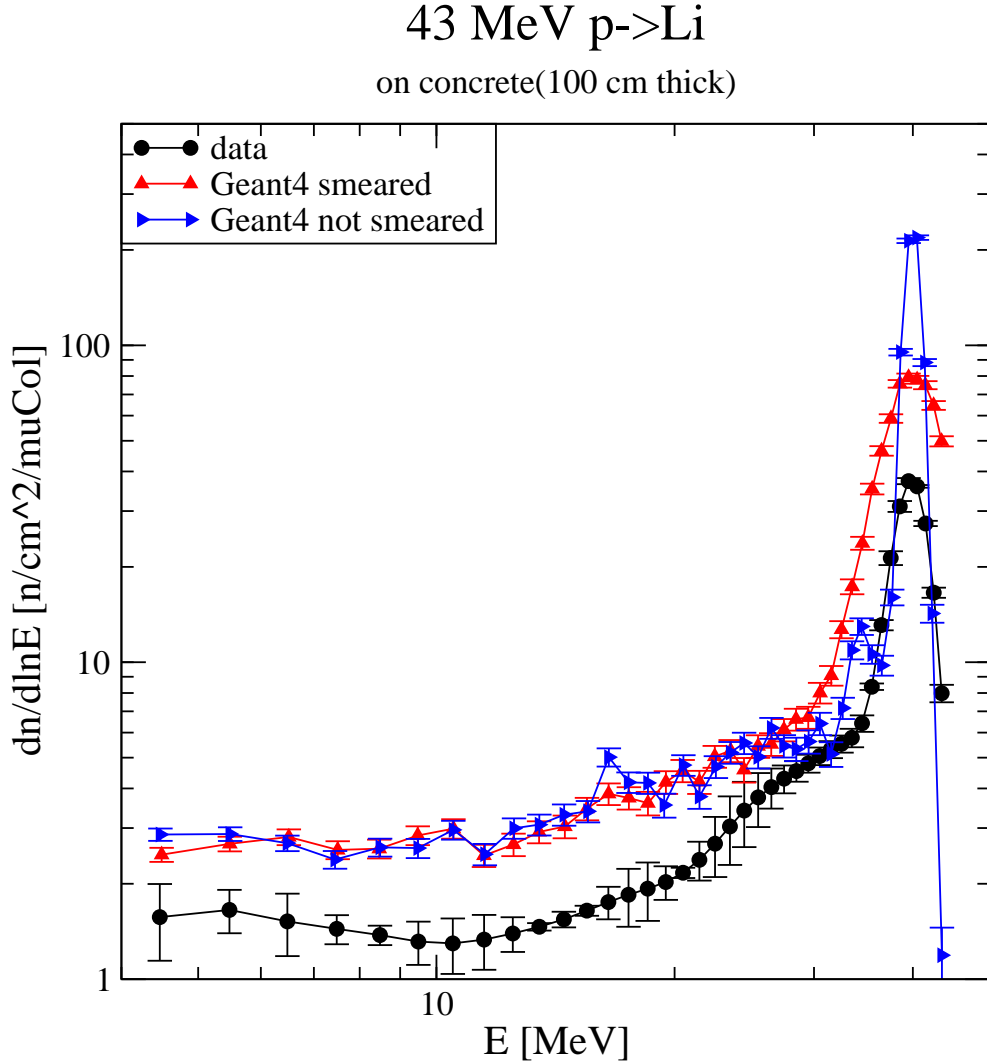


Figure 18: Comparison of neutron energy spectra through 100 cm of concrete shield on beam axis from simulations with and without smearing for 43 MeV $p\text{-}^7\text{Li}$ neutrons. Experimental data are taken from [9].

taken for estimating the flux have been modified according to a Gaussian distribution. For the mean value the calculated neutron energy E was used. The standard deviation σ has been calculated according to the following formula:

$$\sigma = E \times \sqrt{a^2 + \frac{b^2}{E}} \quad (4)$$

Shield Width	Experimental or a Simulation	10 - 35 MeV		35 - 45 MeV	
		Flux [$\frac{n}{cm^2\mu C}$]	$\frac{Sim.}{Exp.}$	Flux [$\frac{n}{cm^2\mu C}$]	$\frac{Sim.}{Exp.}$
100 cm	Exp	3.34E+00	–	5.04E+00	–
	MORSE	5.67E+00	1.70	6.01E+00	1.19
	Geant4 not smeared	5.73E+00	1.72	1.68E+01	3.33
	Geant4 smeared	6.52E+00	1.95	1.50E+01	2.98

Table 7: Comparing the energy fluxes and ratios of simulated to experimental fluxes for Geant4 simulations applying and not applying smearing for ^7Li neutrons and the 100 cm concrete shield.

with E in MeV, $a = 0.05$ and $b = 0.4$. The parameters of the smearing function had to be assumed since they are not given in [9]. The main focus of this note is the comparison of the FOM in two energy regions: below the peak and the peak region. Table 7 shows that the smearing does not change the integrated fluxes in this regions significantly; therefore the comparison of FOM values is not effected much by not taking the detector resolution into account. In all other distributions and values obtained by Geant4 in this report smearing has not been applied. The shape of the distribution (figure 18) changes. The peak becomes smaller and wider. This should be remembered when looking at the other distributions shown in this note.

5 Conclusion

The design of flexible and general implementations of geometrical importance sampling and a scoring system for controlling the importance sampling performance has been presented. The efficiency of the variance reduction technique has been demonstrated for a typical neutron shielding benchmark experiment. A maximal factor in the gain of computing time of about 89 compared to the analog simulation has been achieved in the case of the 68 MeV ^7Li neutrons bombarding the 200 cm concrete shield in the energy region below the peak. The estimated mean values obtained by the Geant4 simulations when using importance sampling agree very well within the errors with the analog simulation showing that the importance sampling implementation does not introduce a bias in the estimated mean values. In some areas large deviations of the simulated results from the experimental data have been encountered. The simulation of these areas should be repeated with upcoming Geant4 versions including improved physics modelling of the neutron energy regions between 20 and 100 MeV. The source code of the simulation is distributed with Geant4 release 5.2 as advanced example: “examples/advanced/Tiara”.

Acknowledgements

The author wishes to thank Noriaki Nakao for the permission to use and include experimental data from the TIARA experiment in this report, John Apostolakis for numerous discussions and suggestions, Gabriele Cosmo for discussions about the design and implementation and

Hans-Peter Wellisch for discussions concerning the hadronic physics.

References

- [1] S. Agostinelli et al.,
Geant4 — a simulation toolkit,
Nucl. Inst. Meth. Phys. Res. A **506** (2003) 250-303.
- [2] By BABAR Computing Group (D.H. Wright et al.),
Using Geant4 in the BABAR Simulation,
e-Print Archive: hep-ph/0305240.
- [3] S. Agostinelli et al.,
Medical applications of the Geant4 Toolkit,
Paper to appear in the Proceedings of the EuroSim 2001 Conference, 2001.
- [4] S. Chauvie et al.,
From HEP computing to biomedical research and vice-versa: technology transfer and
application results,
Proceedings of CHEP2001, Beijing, 2001.
- [5] Kahn H.,
Use of different Monte Carlo sampling techniques,
Symposium on Monte Carlo Methods, ed Meyer H. A., 146-190, New York, Wiley, 1956.
- [6] Hammersley J. M., Handscomb D. C.,
Monte Carlo Methods,
London: Methuen & CO LTD, 1965.
- [7] McGrath E. J., Irving D. C.,
Variance Reduction,
ORNL-RSIC-38 Report,
Techniques for Efficient Monte Carlo Simulation, Vol. III,
Oak Ridge National Laboratory, Oak Ridge (1975).
- [8] Ivan Lux, Laszlo Koblinger,
MONTE CARLO PARTICLE TRANSPORT METHODS: NEUTRON *and* PHOTON
CALCULATIONS,
CRC Press, Inc 1991.
- [9] Noriaki Nakato et al.,
Transmission Through Shields of Quasi-Monoenergetic Neutrons Generated by 43- and
68-MeV Protons—I: Concrete Shielding Experiment and Calculation for Practical Ap-
plication,
Nuclear Science and Engineering **124** (1996) 228-242.

- [10] Thomas E. Booth,
A Sample Problem for Variance Reduction in MCNP,
Los Alamos LA-10363-MS (1985).
- [11] Judith F. Briesmeister, Editor,
MCNPTM - A General Monte Carlo N-Particle Transport Code, Version 4C,
LA-13709-M 18. December 2000.
- [12] Internet page,
Currently at: <http://idsun1.kek.jp/nakao/research/tiara/tiara.htm>.
- [13] J.P. Wellisch,
Hadronic shower models in Geant4 – the frameworks,
Comp. Phys. Comm. **140** (2001) 65-75.
- [14] J.P. Wellisch,
Private communication.